Bioorganic Chemistry 85 (2019) 337–348

Contents lists available at ScienceDirect

Bioorganic Chemistry

journal homepage: www.elsevier.com/locate/bioorg

Synthesis and biological evaluation of some novel thiobenzimidazole derivatives as anti-renal cancer agents through inhibition of c-MET kinase

Hany S. Ibrahim[a,*], Mohamed E. Albakri[a], Walaa R. Mahmoud[b], Heba Abdelrasheed Allam[b], Ahmed M. Reda[c], Hatem A. Abdel-Aziz[d]

[a] Department of Pharmaceutical Chemistry, Faculty of Pharmacy, Egyptian Russian University, Badr City, Cairo 11829, Egypt
[b] Department of Pharmaceutical Chemistry, Faculty of Pharmacy, Cairo University, Cairo 11562, Egypt
[c] Department of Biochemistry, Faculty of Pharmacy, Egyptian Russian University, Badr City, Cairo 11829, Egypt
[d] Department of Applied Organic Chemistry, National Research Center, Dokki, Giza, P.O. Box 12622, Egypt

ARTICLE INFO

Keywords:
Benzimidazole
Renal cell carcinoma
c-Met kinase

ABSTRACT

Benzimidazole is an interesting scaffold constituting a main core in many anticancer agents against variable cell lines as Carbendazim (**I**) and Nocodazole (**II**). Accordingly, eighteen compounds of 2-((1H-benzoimidazol-2-yl) thio)-1-(aryl/heteroaryl)ethan-1-ones, in their sulfate salt and free forms, were designed and investigated as anticancer agents. *In vitro* preliminary screening of selected compounds by the National Cancer Institute (NCI) on a panel of 60 cell lines revealed renal cancer cell line (A498) as the most vulnerable cell line; accordingly, IC_{50} values against A498 cell line were determined for compounds with the best results. The best inhibitory activity was for compound **4a** with (IC_{50} = 6.97 μM) compared to sunitinib as a reference drug (IC_{50} = 6.99 μM). Compound **4a** was further subjected to cell cycle analysis that indicated the decrease in cell population in the G2/M phase when compared to the untreated control cells. In addition, it showed significant increase in the late apoptosis in Annexin-V FTIC study compared to the control cells. An enzymatic inhibitory study on compound **4a** against c-Met and MAP kinases revealed its better activity against c-Met kinase with (IC_{50} = 0.27 μM) compared to sunitinib (IC_{50} = 0.18 μM). Molecular docking study was conducted to reveal the interactions of compound **4a** in the active site of c-Met kinase. Computational ADME study was performed to insure that compound **4a** has proper pharmacokinetic and drug-likeness properties.

1. Introduction

Cancer is the second deadly disease worldwide according to WHO. Among different types of cancer, kidney cancer is the world's sixteenth reason of cancer death as it is responsible for 1.7% of all death rate worldwide and it shares 2.4% of total cancer patients around the world [1–3]. Kidney cancer is among the 10 most common cancers in both men and women and it is has high incidence rate in many countries among them Czech Republic and North America [4,5].

On the other hand, the anticancer activity of benzimidazole derivatives is well established against different cancer types [6–8]. For example, methyl-2-benzimidazole carbamate (Carbendazim, FB642, **I**) (Fig. 1), an anticancer agent in preclinical trials, exerted an apoptotic effect by inhibition of microtubules against both colon cancer cell lines (HT-29) and murine B16 melanoma [6,7]. Another methyl-2-benzimidazole carbamate derivative (Nocodazole, NSC-238189, **II**) interferes with the microtubules and affects many cancer cells by inhibition of several kinases as MET, AB1 and C-KIT [8]. Dovotinib, (**III**) can target multiple RTK enzymes such as FLT3, VEFGR, C-Kit and PDGFR with IC_{50} values = 1, 65, 2 and 5 nM, respectively [9,10]. It is used for patients with gastrointestinal stromal tumor resistant to imatinib [11]. A bicyclic benzimidazole derivative (BMT-1, **IV**) (Fig. 1) activates several mechanisms to induce apoptosis in multiple myeloma cells including the activation of caspase-3, caspase-8 and caspase-9 [12]. Similarly, compound (**V**) was found to be cytotoxic against UO31 renal cancer cell line with inhibitory activity against c-MET kinase up to 82% at conc. = 10 μM [13]. 2-Tolyl benzimidazole derivatives (**VI**) (Fig. 1) displayed cytotoxicity and apoptotic activity against MDA-MB-468 breast cancer cell line, with high expression for EGFR, by IC_{50} = 3.31 μM [12].

To be more specific in this aspect, incorporation of acetophenone moieties with 2-thiobenzimidazole as shown in compounds **VII** and **VIII** (Fig. 1) resulted in significant cytotoxic activity. Compound **VII** inhibited 50% of cell surface expression of CD-133 on HT-29 cancer cell line at conc. = 10 μM [14] while compound **VIII** caused cell cycle arrest

* Corresponding author.
E-mail address: Hany.s.ibrahim@gmail.com (H.S. Ibrahim).

https://doi.org/10.1016/j.bioorg.2019.01.006
Received 5 November 2018; Received in revised form 27 December 2018; Accepted 6 January 2019
Available online 08 January 2019
0045-2068/

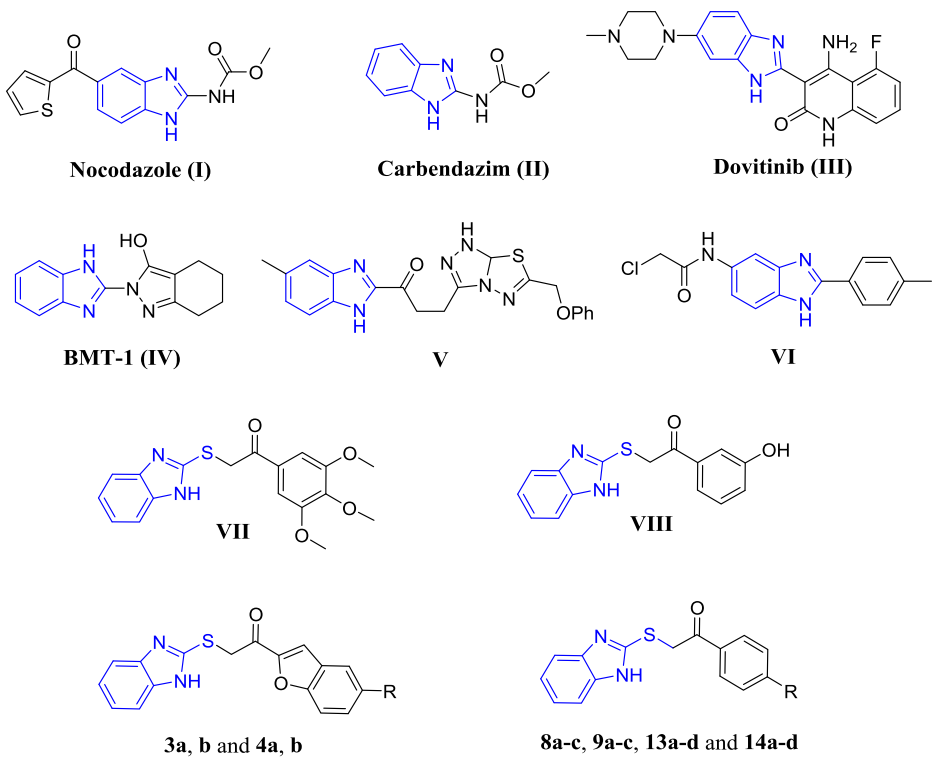

Fig. 1. Reported benzimidazole and 2-thiobenzimidazole anticancer agents, and the scaffold of the target compounds.

and apoptosis of MDA-MB-468 cancer cell line [15].

In this research, we report the synthesis of new 2-thiobenzimdazole derivatives combined with different acetophenones (**4a-b**, **9a-c** and **14a-d)** and their corresponding sulfate salt analogues (**3a-b**, **8a-c** and **13a-d)** to be investigated for their cytotoxic activity followed by some mechanistic studies to explain their biological activity. Furthermore, molecular docking study was conducted to draw the full picture about the mechanism of action of the anticancer activity of the synthesized compounds.

2. Results and discussion

2.1. Chemistry

We report herein the synthesis of novel 2-substituted benzimidazol-3-ium sulfate compounds and their free analogues following three different schemes starting from different ketones (Schemes 1–3). In Scheme 1, cyclization of salicylaldehyde (**1a**) or 5-bromosalicylaldehyde (**1b**) with chloroacetone in the presence of potassium hydroxide yielded the corresponding 2-acetylbenzofurans **2a**, **b** [16]. Reaction of compounds **2a**, **b** with 2-mercaptobenzothiazole in the presence of two equivalents of conc. sulfuric acid according to the modified method reported by Abdel-Aziz et al. [14] gave 2-substituted thiobenzimidazole sulfate salts **3a**, **b** in 88 and 90% yields, respectively. The structure of the latter isolated sulfate salts was supported by the reported X-ray crystal structure of similar salts [14,17]. Liberation of the free compounds from the sulfate salts was done by neutralization *via* stirring with sodium bicarbonate solution at room temperature to furnish the corresponding free bases **4a**, **b**.

Secondly, in Scheme 2, 4-aminoacetophenone (**5**) is converted into the corresponding 4-phenylurido-acetophenones **7a**, **b** [18] by the

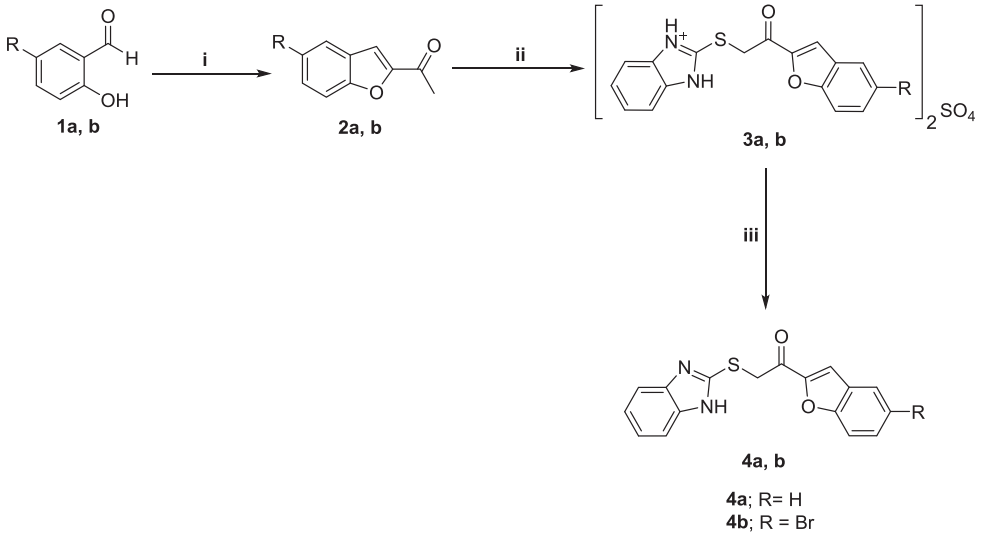

Scheme 1. **(i)** chloroacetone, KOH, methanol, reflux, 15 min.; **(ii)** 2-mercaptobenzimidazole, H_2SO_4, AcOH, reflux 1 h; **(iii)** Na_2CO_3, stirring, rt., 24 h.

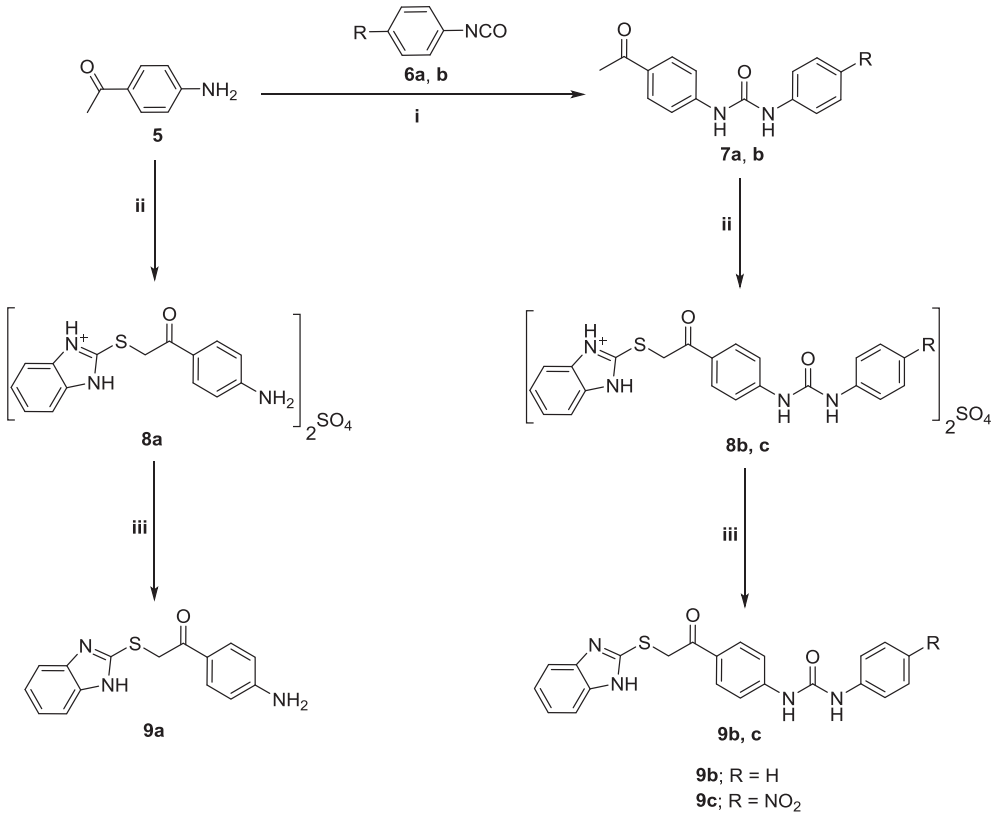

Scheme 2. (i) dry toluene, reflux, 24 h; **(ii)** 2-mercaptobenzimidazole, H_2SO_4, AcOH, reflux 1 h; **(iii)** Na_2CO_3, stirring, rt., 24 h.

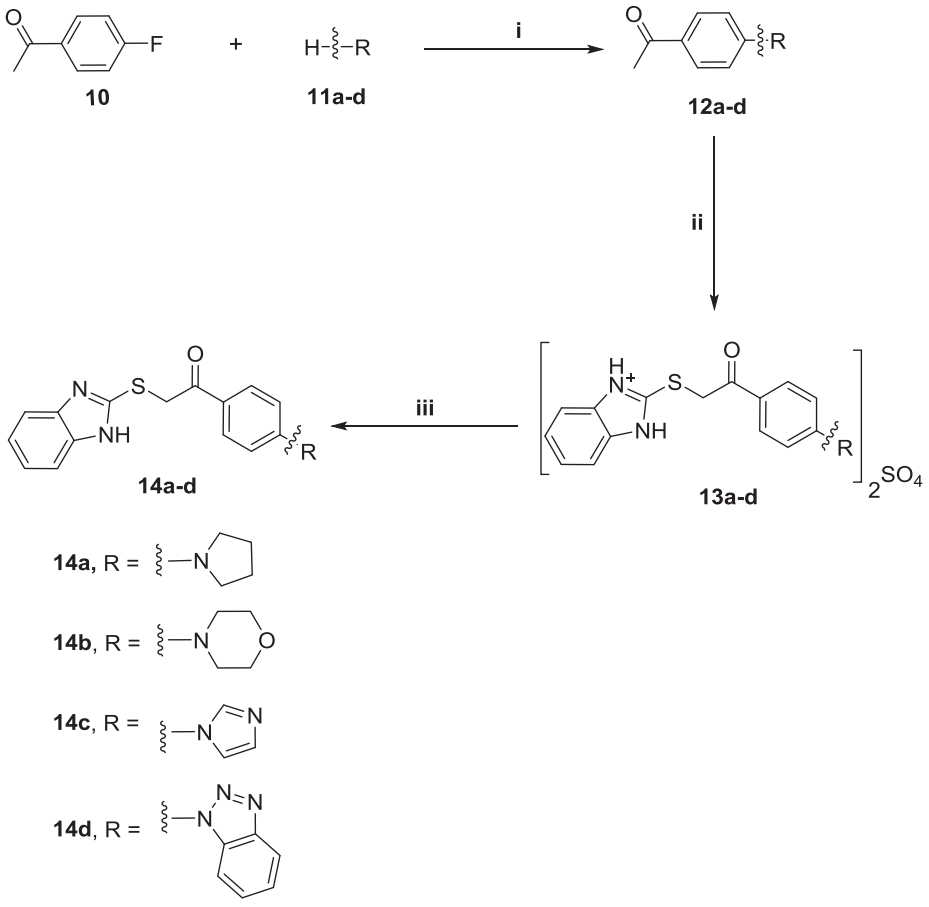

Scheme 3. (i) K_2CO_3, DMSO, reflux, 3–5 h; **(ii)** 2-mercaptobenzimidazole, H_2SO_4, AcOH, reflux 1 h; **(iii)** Na_2CO_3, stirring, rt., 24 h.

reaction of the appropriate isocyanate **6a**, **b**. The reaction of **5** or **7a**, **b** with 2-mercaptobenzimidazole gave the corresponding sulfate salts **8a-c** and then the corresponding free analogues **9a-c** applying the same procedure adopted in Scheme 1. The ^{1}H NMR spectra of **8a** and **9a** revealed the singlet signal at 5.34 and 4.87 ppm, respectively, assigned for the two protons of the CH_2 group. It's worthy to mention that applying the same steps using five equivalents of conc. sulfuric acid afford the previously reported thiazolobenzimidazole sulfate salt [17].

In Scheme 3, pyrrolidine (**11a**), morpholine (**11b**), 1*H*-imidazole (**11c**) or 1*H*-benzo[*d*][1,2,3]triazole (**11d**) were reacted with 4-fluoroacetophenone (**10**) to yield *4*-substituted-acetophenones **12a-d** [19] which were then subjected to the same procedure to afford the sulfate salts **13a-d** and then free bases **14a-d**.

2.2. Biological evaluation

2.2.1. In vitro anticancer activity as primary single high dose (10^{-5} M) screening

The structure of the synthesized compound **8c** was selected by the NCI Developmental Therapeutic Program (www.dtp.nci.nih.gov) for evaluation of its cytotoxic activity against a panel of sixty cancer cell lines at concentration 10^{-5} M. The anticancer assays were performed in accordance with the protocol of the Drug Evaluation Branch, NCI, Bethesda [38–40].

The obtained results in Fig. 2 revealed that, compound **8c** possessed the highest cytotoxic activity against renal cancer cell line A498 with GI % = 59. This result was the starting point to investigate the anticancer activity of the other synthesized compounds against A498 cancer cell lines.

2.2.1.1. In vitro cytotoxic activity against renal cancer cell line A498. The previous results motivated us to investigate the cytotoxic activity for all the synthesized compounds against renal cancer cell line A498 as shown in Table 1. Cell viability for A498 was measured upon treatment with all the compounds except **8c** (previously screened by NCI) at conc. 10 μM. The results revealed that compounds **4a**, **9a** and **9c** in addition to their corresponding salts **3a**, **8a** and **8c** displayed the most cytotoxic effects (Table 1). Consequently, IC_{50} values for these compounds were calculated to evaluate anticancer effect on A498 cancer cell line. Compound **4a** possessed the best IC_{50} value among all the tested compounds (IC_{50} = 6.97 μM) with respect to the reference drug sunitinib (IC_{50} = 3.99 μM). According to the given results, it was discovered that combination of 2-thiobenzimidazole with 2-acetylbenzofuran and 4-aminoacetophenone will lead to the maximum cytotoxic activity against A498.

2.2.1.2. Structure activity relationship (SAR). Cytotoxic activity on renal cancer cell line A498 revealed that both salt and free compound for the same derivative showed near activity. Based on the used acetyl derivative in each compound, SAR studies showed benzofused heterocyclic acetyl derivative, as 2-acetylbenzofuran in compounds **3a** and **4a** yield the maximum cytotoxicity (**4a**; IC_{50} = 6.97 μM) while addition of 5-bromo substituent to this group would abolish the activity. On the other hand, according to different *p*-susbtituted acetophenones were combined with 2-thiobenzimidazoles, using *p*-amino group, as compound **8a**) would result a moderate activity with IC_{50} = 11.64 μM. Cyclization of this amino group as in secondary aliphatic amines as in compounds (**13a-d** and **14a-d**) would decrease or abolish the activity. Moreover, phenyl urea extension of this amino group would abolish the activity as in compounds (**8b** and **9b**). Addition of nitro group to phenyl urea extension as in compounds (**8c** and **9c**) would retain weak cytotoxic activity (**8c**; IC_{50} = 36.77 μM).

Table 1
Cytotoxic activity of the synthesized compounds against renal cancer cell line A498.

Compound	Cytotoxicity against A498	
	% Cell viability at 10 μM	IC_{50} (μM)
3a	25.93	7.12 ± 0.08
3b	88.06	———
4a	20.89	6.97 ± 0.87
4b	70.76	———
8a	35.87	11.64 ± 1.13
8b	100	———
8c	——	36.77 ± 0.92
9a	36.87	12.5 ± 0.76
9b	100	———
9c	36.72	39.79 ± 1.04
13a	65.69	———
13b	55.90	———
13c	100	———
13d	91.72	———
14a	78.09	——
14b	85.77	———
14c	100	———
14d	100	———
Sunitinib	–	3.99 ± 0.14

2.2.2. Flow cytometric analysis and apoptotic studies

Compound **4a** was the most cytotoxic compound against A498 cancer cell line; accordingly, flow cytometric analysis was established to study its effect on the cell cycle phases in the same cancer cell line. In addition, apoptotic activity were measured by Annexin V-based flow cytometric analysis.

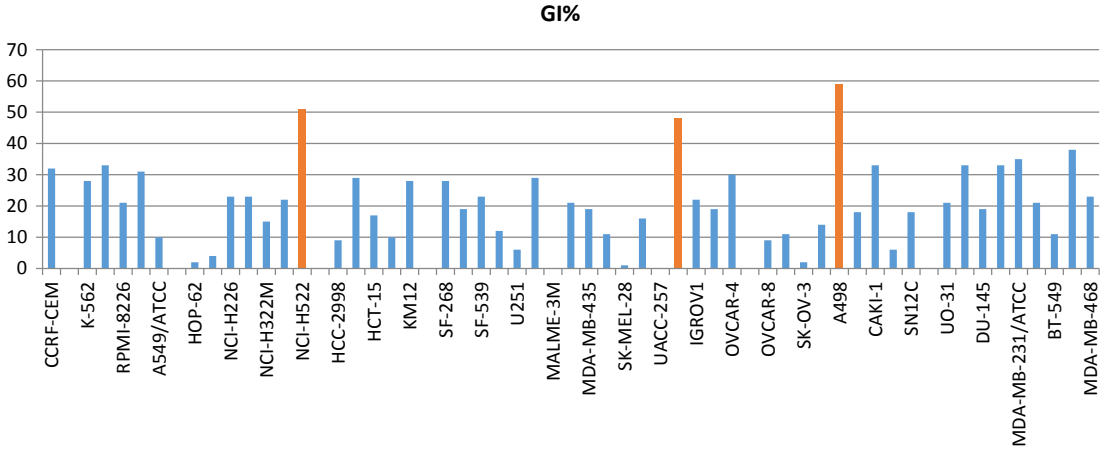

Fig. 2. Percentage growth inhibition (GI %) of *in vitro* subpanel tumor cell lines at 10 μM concentration for compound **8c**.

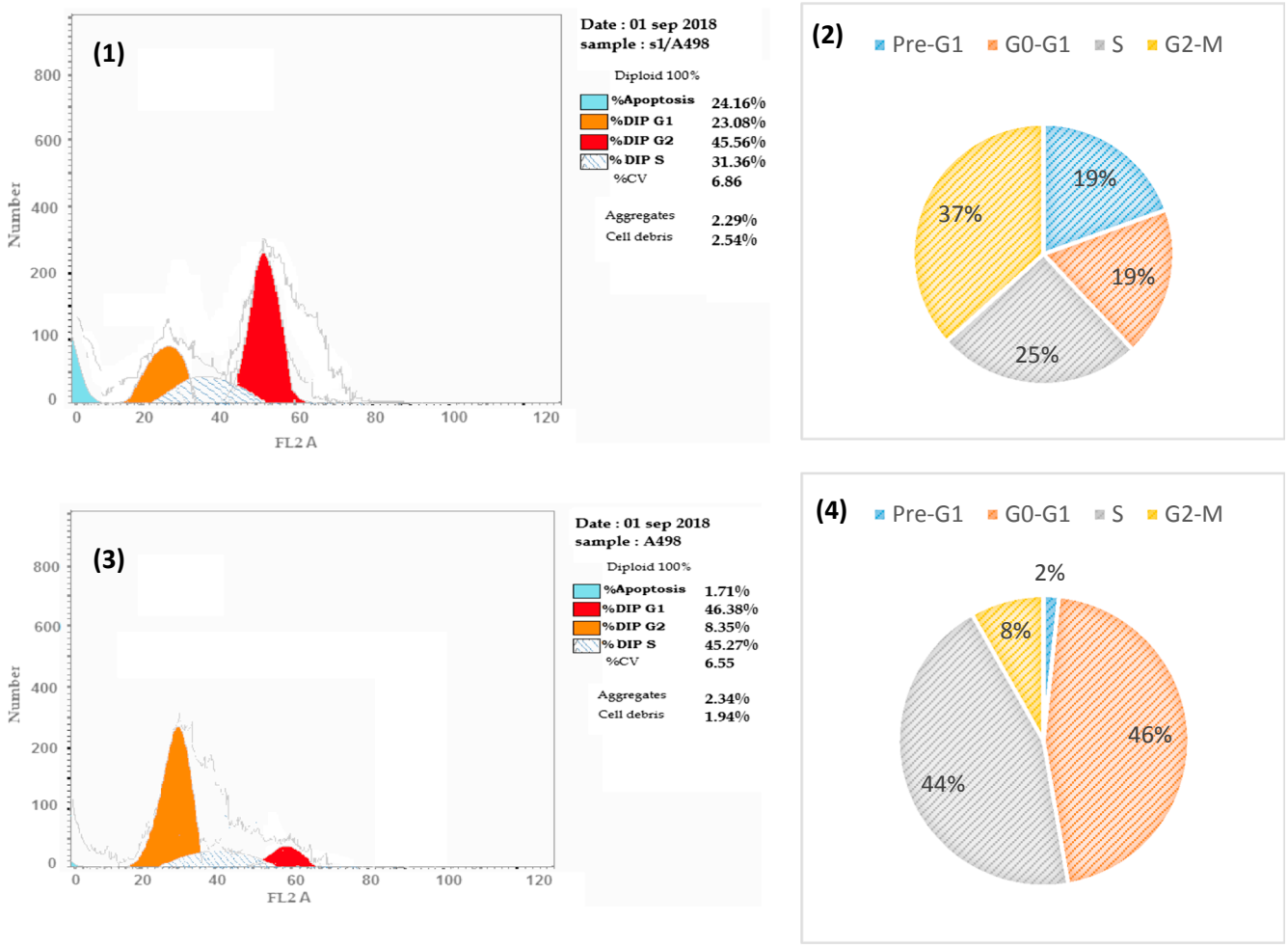

Fig. 3. (1) Flow cytometric analysis of A498 cancer cell lines treated with compound **4a** at concentration equals to its IC_{50} on the same cell line. **(2)** Pie chart to illustrate the % of each stage of the cell cycle of the same case in (1). **(3)** Flow cytometric analysis of A498 cancer cell lines without any treatment. **(4)** Pie chart to illustrate the % of each stage of the cell cycle of the same case in (**3**).

2.2.2.1. Cell cycle analysis. In this part, cancer cell line A498 was treated with compound **4a** with concentration equals to its IC_{50} (6.97 μM). Fig. 3 revealed that compound **4a** could disrupt the normal cell cycle by decreasing G0-G1 phase by approximately 0.4 folds and S phase by approximately 0.5 folds with respect to the control. On the other hand, Pre-G and G2/M phase of the treated cell was increased by 9.5 folds and 4.6 folds relative to the control. As a result, this disruption in cell cycle which leads to arrest in G2/M phases was considered as a significant marker for induction of apoptosis [20–22].

2.2.2.2. Annexin-V FTIC apoptotic study. To assure the apoptotic effect of compound **4a**, Annexin-V FTIC/PI dual staining assay was established with IC_{50} concentration on A498 cancer cell line. Analysis of the results in Fig. 4 declared the apoptotic effect of compound **4a** by showing a significant increase in the percent of positive apoptotic cells in (UR + LR) corners from 1.4% to 21.11% which comprises about 15 fold with respect to control (Fig. 4).

*2.2.3. Inhibitory activity of compound **4a** against c-MET and MAP kinases*

In order to acquire more details about the mechanism regarding the cytotoxic activity of compound **4a** against A498 cancer cell line, literature survey informed us with very interesting information that c-Met (hepatocyte growth factor receptor which is encoded by the met gene) and MAPK (mitogen activated protein kinase) are highly expressed in A498 cancer cells [23,24]. For this reason, compound **4a** was evaluated for its inhibitory activity against both enzymes using sunitinib as a reference drug as shown in Table 2. The given results revealed that the inhibitory activity of compound **4a** (IC_{50} = 0.27 μM) against c-MET kinase is very close to the reference drug sunitinib (IC_{50} = 0.18 μM). On the other hand, compound **4a** showed weak activity against MAPK (IC_{50} = 1.01 μM) compared to the reference drug sunitinib (IC_{50} = 0.64 μM) (Table 2).

3. *In silico* studies

3.1. Molecular docking study

Molecular docking simulations of compound **4a** inside the active site of c-MET kinase was established in order to get more information about the mode of interaction that leads to the given inhibitory activity. Docking simulation was performed using Accelrys Discovery Studio 4 using the crystal structure of c-Met kinase with PDB code (3ZZE) (Res. 1.87 Å) in which the main group of co-crystalized ligand was oxindole. Therefore, analogy of the structure of the co-crystalized ligand [25] and

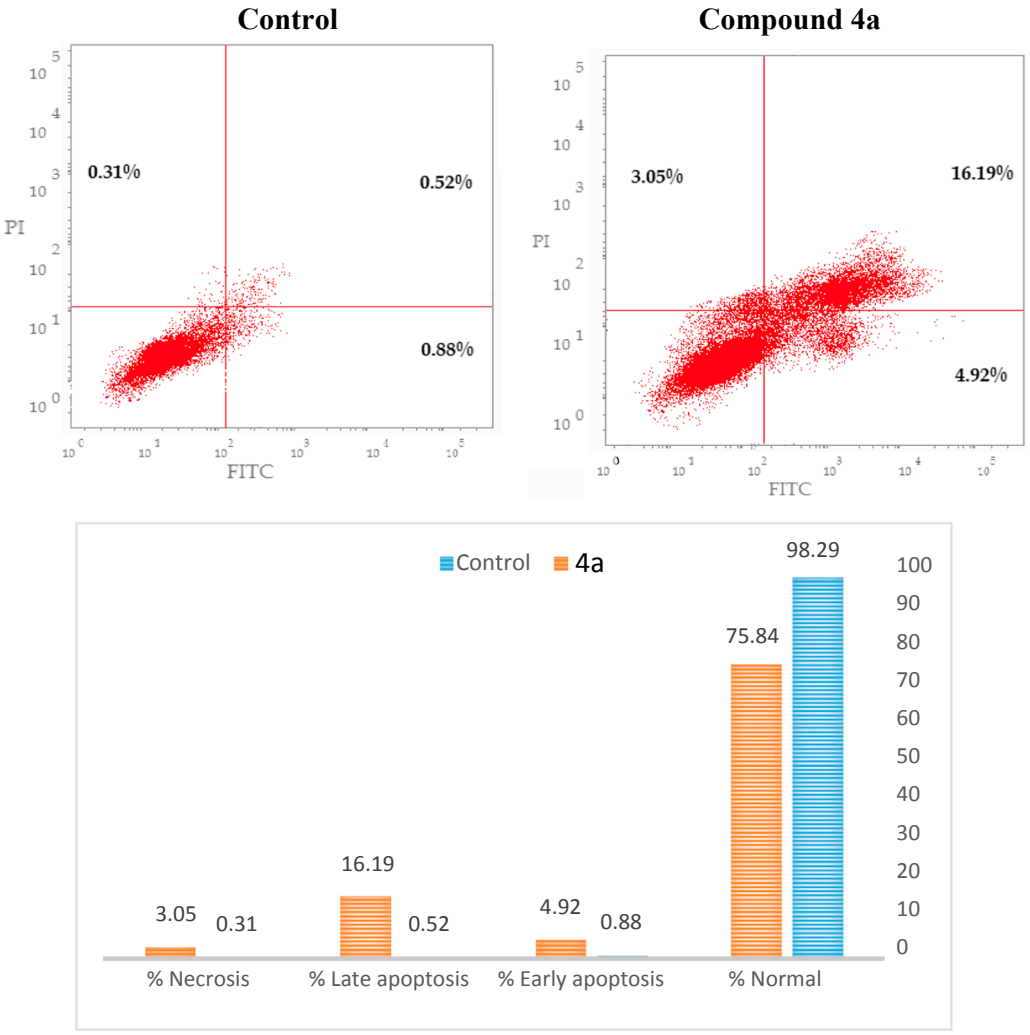

Fig. 4. Apoptotic effect of compound **4a** on renal cancer cell lines A498 that was illustrated through Annexin V-FTIC positive staining technique. The four quadrants is known as (LL: viable, LR: early apoptosis, UR: late apoptosis, UL: necrosis).

Table 2
Inhibitory effect of both compound **4a** and the reference drug sunitinib against both c-MET and MAP kinases.

Compound	IC_{50} (μM)	
	c-MET	MAPK
4a	0.27 ± 4.28	1.01 ± 8.7
Sunitinib	0.18 ± 1.99	0.64 ± 5.05

compound **4a** can be revealed by the interact of both of them with two amino acids R1208 (1.9 Å) and D1222 with 2 hydrogen bonds (2.5 Å) (Fig. 5a). Additionally, the benzofuran moiety was engulfed by the hydrophobic pocket consisted of V1092, A1108, M1160 and M1211 (Fig. 5b).

3.2. ADME study and pharmacokinetic properties prediction

In order to have an overview on the pharmacokinetic aspects of the biologically promising candidate **4a**, the physical properties, the ADME parameters as well as the pharmacokinetic profile of compound **4a** were computed using the freely accessible web server SwissADME (http://swissadme.ch/index.php#undefined) where it revealed promising physicochemical and pharmacokinetic properties (Fig. 6). It exhibited a predicted consensus log Po/w value of 3.48 with moderate water solubility, high GIT absorption and no BBB permeability, which correlates with minimal predicted CNS adverse effects. In addition, Fig. 6 showed that compound 4a achieve all the conditions of drug-likeness characters however, it cannot be classified as lead-like as XLOGP3 model is more than 3.5.

The BOILED-Egg chart of compound **4a** relating WLOGP and TPSA [26] (Fig. 7) indicated its high probability to be passively absorbed by the gastrointestinal tract with no BBB permeability. The chart also clarified that compound **4a** is not a substrate for the P-glycoprotein (PGP-) and thus eliminating the possibility of its resistance by tumor cell lines through efflux. Fig. 8 shows the oral bioavailability radar chart of compound **4a** taking into consideration the six key criteria controlling the oral bioavailability [27,28] where the optimal values are represented as a pink area with the tested compound is presented as red line therein. As shown in Fig. 8, compounds which is nearly fully included in the pink area (except saturation (INSATU) property) indicating its good predicted oral bioavailability, with promising pharmacokinetic properties.

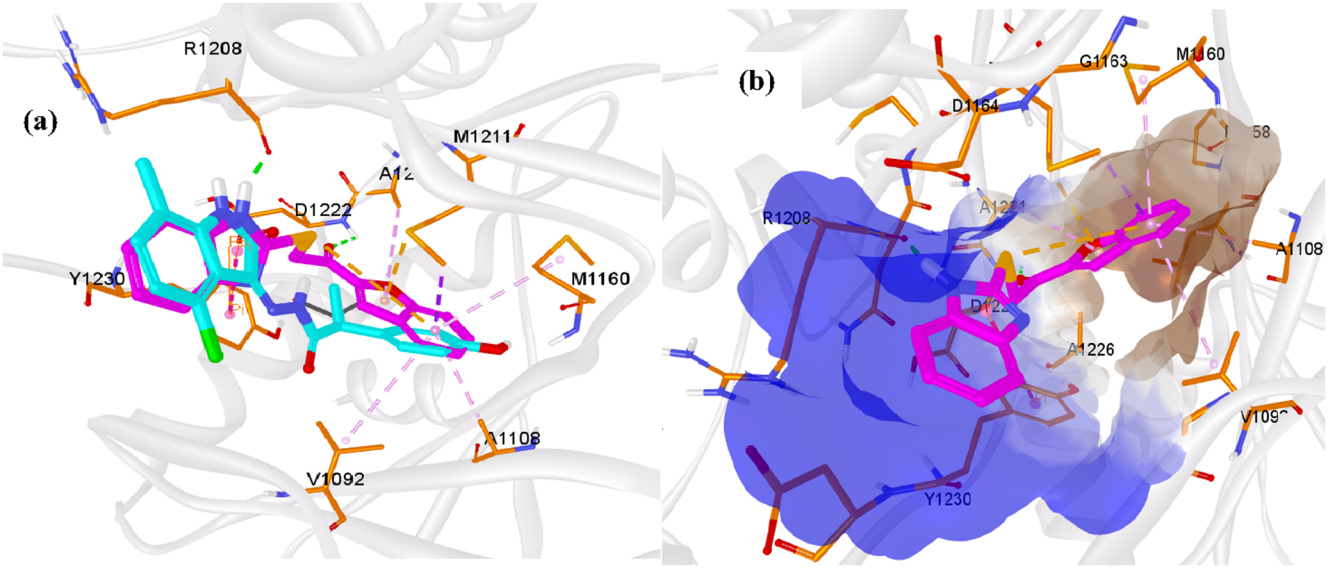

Fig. 5. **(a)** Alignment of co-crystallized ligand (carbons were colored as cyan) and compound **4a** (carbons were colored as violet) in the active site of c-Met kinase (PDB code 3ZZE) showing the main interaction with the key amino acids in the active site. (**b**) Compound **4a** in the active site of c-Met kinase surrounded by a pocket showing the hydrophobic interaction. Color gradient from brown (hydrophobic) to blue (hydrophilic). Color scheme; hydrogen bonds, Pi-Pi interactions, hydrophobic interactions were assigned as green, orange and purple dots, respectively.

4. Conclusion

Eighteen derivatives of 2-substituted thiobenzimidazoles with different acetophenone moieties were synthesized and screened for their anticancer activity against renal cancer cell line A498. Among the tested compounds, the best IC_{50} value was for compound **4a** with (IC_{50} = 6.97 μM) compared to sunitinib as reference drug (IC_{50} = 6.99 μM). Moreover, cell cycle analysis of compound **4a** revealed its relevant decrease in cell population in the G2/M phases as well as late apoptotic induction effect as demonstrated from Annexin-V

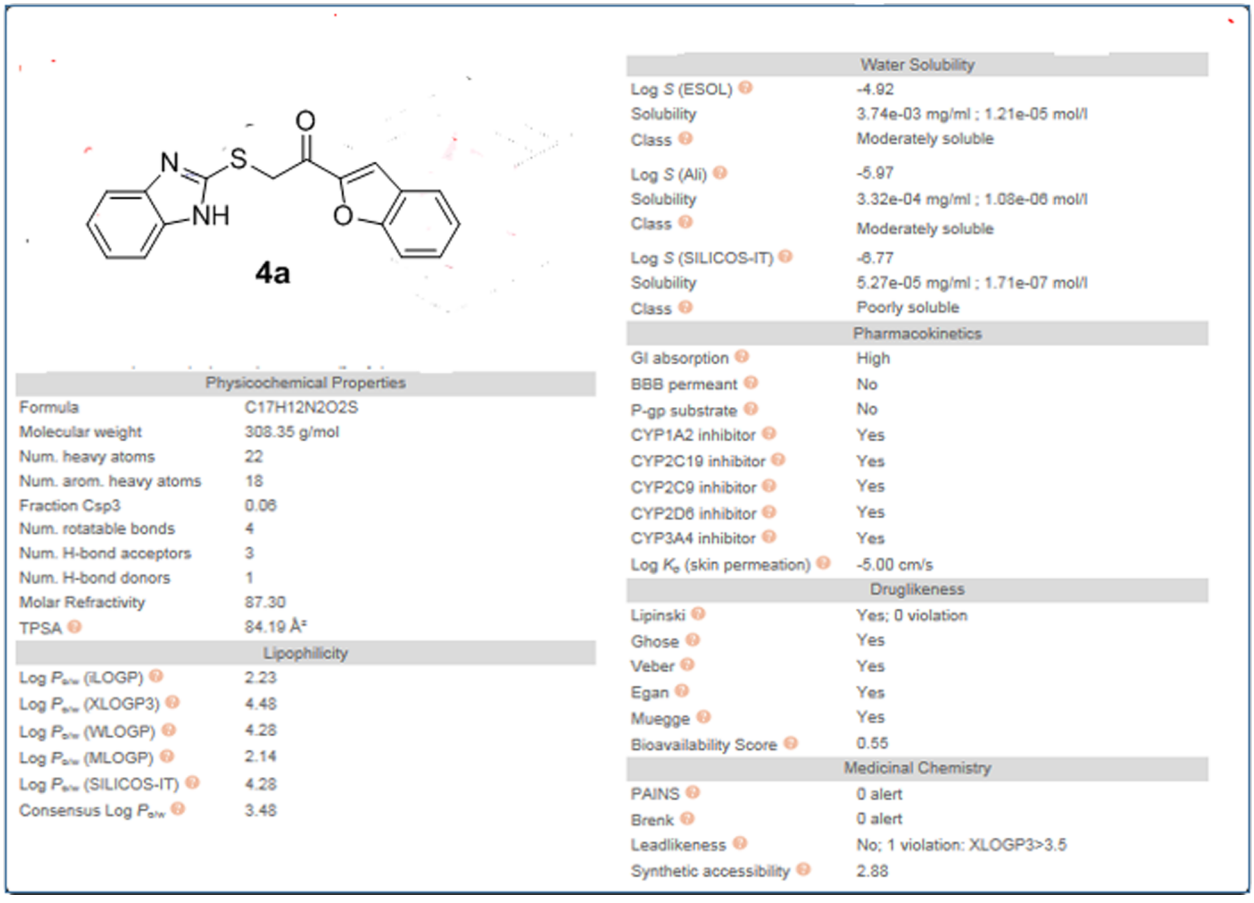

Fig. 6. The pharmacokinetic profile of compound **4a** from SwissADME web server.

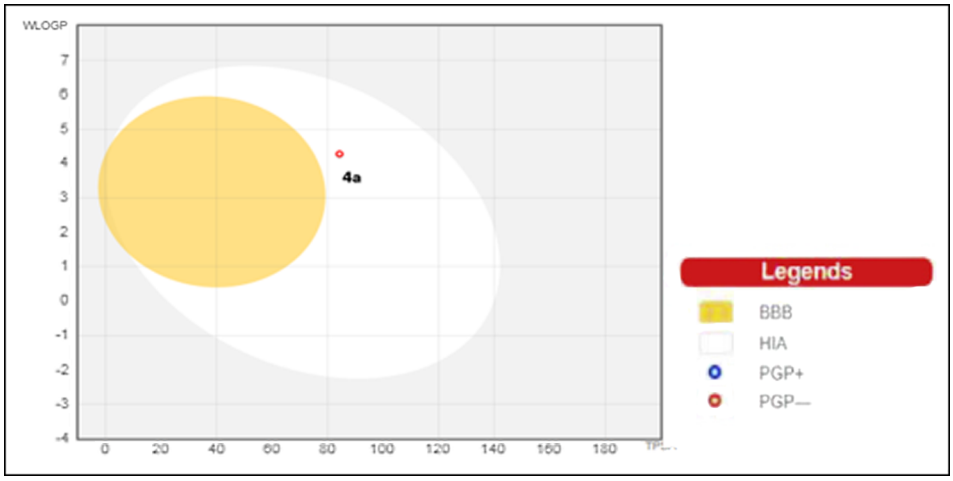

Fig. 7. The BOILED-Egg chart for compound **4a** developed by swissADME.

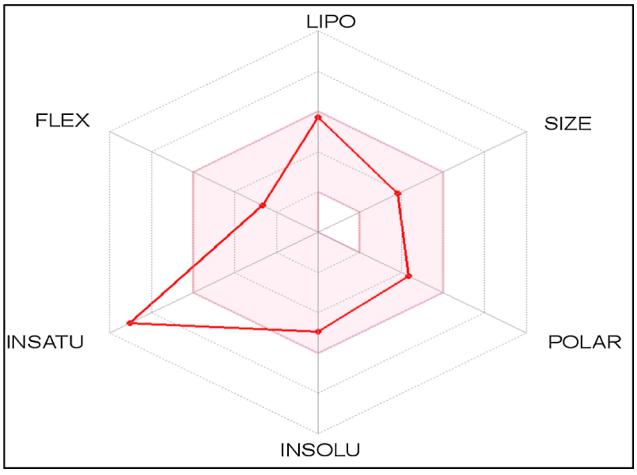

Fig. 8. Bioavailability radar chart for compound **4a**. The pink area represents the range of the optimal property values for oral bioavailability and the red line is compound **4a** predicted properties. Saturation (INSATU), size (SIZE), polarity (POLAR), solubility (INSOLU), lipophilicity (LIPO) and flexibility (FLEX).

FTIC study. Applying an enzymatic inhibitory study of compound **4a** against c-Met and MAP kinases showed its superior activity against c-Met kinase with (IC_{50} = 0.27 μM) compared to sunitinib (IC_{50} = 0.18 μM). Finally, the obtained results were supported by a molecular docking study of compound **4a** pointing out its possible interactions at the active site of c-Met kinase enzyme. Compound **4a** illustrated suitable pharmacokinetic properties that was proved by swissADME server.

5. Experimental

5.1. Chemistry

5.1.1. General

Melting points were recorded on a Stuart SMP10 digital melting point apparatus and were uncorrected. Infrared and NMR spectra were performed at the Microanalytical Unit-Faculty of Pharmacy, Cairo University. IR Spectra were recorded as KBr disks using a Shimadzu FT-IR 8400S infrared spectrophotometer. Mass spectral data are given as *m/z* (Intensity %). NMR spectra were recorded on a Bruker Ascend 400/R (^{1}H: 400, ^{13}C: 100 MHz) spectrometer. ^{1}H NMR spectra were run at 400 MHz and ^{13}C spectra were run at 100 MHz in deuterated dimethylsulfoxide (DMSO-d_6). Chemical shifts are expressed in δ values (ppm) using the solvent peak as internal standard. All coupling constant (J) values are given in hertz. The abbreviations used are as follows: s, singlet; d, doublet; m, multiplet. Elemental analyses were carried out at the Regional Center for Mycology and Biotechnology, Al-Azhar University, Egypt. Thin Layer Chromatography (TLC) routinely monitored reaction progress on silica gel pre-coated F254 Merck plates. Unless otherwise noted, all solvents and reagents were commercially available and used without further purification. The acetophenone intermediates **2a**, **2b** [16], **6a** [18], **6b** [18], **12a-d** [19,29] were synthesized according to the reported procedures.

5.1.2. General procedure for preparation of sulfate salts

To a solution of the appropriate acetophenone (5 mmol) in 10 mL glacial acetic acid, 2-mercaptobenzimidazole (0.75 g, 5 mmol) and conc. sulphuric acid (10 mmol) were added. The reaction mixture was heated under reflux for half to two hours. The solid product obtained upon cooling was filtered off, washed with cold water then with petroleum ether and recrystallized from ethanol to afford the corresponding sulfate salts.

5.1.2.1. 2-[(2-(Benzofuran-2-yl)-2-oxoethyl)thio]-1H-benzo[d]imidazol-3-ium sulfate ***3a***. Buff powder, (yield 88%), m.p. 214–215 °C; IR (KBr, ν cm^{-1}): 3400 (NH) and 1666 (C=O); ^{1}H NMR (DMSO-d_6) δ *ppm*: 5.14 (s, 4H, 2C$\underline{H}_2$), 7.13–7.14 (m, 2H, Ar–H), 7.36–7.39 (m, 4H, Ar–H), 7.41–7.45 (m, 2H, Ar–H), 7.59–7.63 (m, 4H, Ar–H), 7.77 (dd, 2H, Ar–H, *J* = 7.6, 7.8 Hz), 7.91 (d, 2H, Ar–H, *J* = 7.8), 8.11 (s, 2H, Ar–H), 12.51 (s, 2H, 2NH, D_2O exchangeable); ^{13}C NMR (DMSO-d_6) δ ppm: 40.61 ($\underline{C}H_2$), 109.94, 112.79, 113.93, 115.91, 122.77, 124.43, 124.57, 124.85, 127.12, 129.54, 132.71, 150.20, 151.02, 155.61, 168.59, 183.36 (C=O); Anal. Calcd. for $C_{34}H_{26}N_4O_8S_3$ (714.79): C, 57.13; H, 3.67; N, 7.84; S, 13.46; Found C, 57.41; H, 3.81; N, 8.09; S, 13.38.

5.1.2.2. 2-[(2-(5-Bromobenzofuran-2-yl)-2-oxoethyl)thio]-1H-benzo[d] imidazol-3-ium sulfate ***3b***. Light yellow powder, (yield 90%), m.p. 220–222 °C; IR (KBr, ν cm^{-1}): 3348 (NH), 1678 (C=O); ^{1}H NMR (DMSO-d_6) δ *ppm*: 5.14 (s, 4H, 2C$\underline{H}_2$), 7.36–7.38 (m, 4H, Ar–H), 7.61–7.62 (m, 4H, Ar–H), 7.73–7.79 (m, 4H, Ar–H), 8.05 (s, 2H, Ar–H), 8.16 (s, 2H, Ar–H), 12.51 (s, 2H, 2NH, D_2O exchangeable); ^{13}C NMR (DMSO-d_6) δ ppm: 40.46 ($\underline{C}H_2$), 113.94, 114.94, 116.97, 121.13, 124.48, 126.71, 128.50, 129.28, 132.07, 135.46, 143.20, 150.05, 151.96, 153.20, 154.33, 183.44 (C=O); Anal. Calcd. for $C_{34}H_{24}Br_2N_4O_8S_3$ (872.58): C, 46.80; H, 2.77; N, 6.42; S, 11.02; Found C, 47.07; H, 2.94; N, 6.58; S, 11.13.

5.1.2.3. 2-[(2-(4-Ammoniophenyl)-2-oxoethyl)thio]-1H-benzo[d] imidazol-3-ium sulfate ***8a***. White powder, (yield 91%), m.p. 198–200 °C;

IR (KBr, ν cm-1): 3470, 3410 (NH) and 1678 (C=O); ^{1}H NMR (DMSO-d_6) δ ppm: 5.34 (s, 2H, C$\underline{H}_2$), 6.68 (d, 2H, Ar−H, J = 7.6 Hz), 7.48–7.51 (m, 2H, Ar−H), 7.70–7.73 (m, 2H, Ar−H), 7.82 (d, 2H, Ar−H, J = 8.4 Hz), 11.10 (s, 1H, NH, D_2O exchangeable); ^{13}C NMR (DMSO-d_6) δ ppm: 41.99 ($\underline{C}H_2$), 113.49, 113.80, 123.09, 125.80, 127.20, 129.99, 130.80, 131.61, 132.57, 151.51, 154.17, 189.30 (C=O); Anal. Calcd. for $C_{15}H_{15}N_3O_5S_2$ (381.43): C, 47.23; H, 3.96; N, 11.02; S, 16.81; Found C, 47.59; H, 4.12; N, 11.38; S, 16.95.

5.1.2.4. 2-[(2-Oxo-2-(4-(3 phenylureido)phenyl)ethyl)thio]-1H-benzo[d] imidazol-3-ium sulfate ***8b***. Buff powder, (yield 87%), m.p. 263–265 °C; IR (KBr, ν cm^{-1}): 3352, 3275 (NHs) and 1654 (C=O); ^{1}H NMR (DMSO-d_6) δ *ppm*: 5.36 (s, 4H, 2C$\underline{H}_2$), 7.01 (t, 2H, Ar−H, J = 7.3 Hz), 7.31 (t, 4H, Ar−H, J = 7.9 Hz), 7.42–7.44 (m, 4H, Ar−H), 7.48 (d, 4H, Ar−H, J = 7.6 Hz), 7.65–7.68 (m, 8H, Ar−H), 8.04 (d, 4H, Ar−H, J = 8.8 Hz), 9.33 (s, 2H, 2NH, D_2O exchangeable), 9.75 (s, 2H, 2NH, D_2O exchangeable), 12.50 (s, 2H, 2NH, D_2O exchangeable); ^{13}C NMR (DMSO-d_6) δ *ppm*: 41.54 ($\underline{C}H_2$), 113.67, 117.51, 118.76, 122.69, 125.03, 127.79, 128.44, 129.31, 130.65, 134.13, 137.50, 139.78, 145.96, 151.02, 152.72, 191.01 (2$\underline{C}$ = O);; ESI MS *m/z*: 903.31 [M]$^+$; Anal. Calcd. for $C_{44}H_{38}N_8O_8S_3$ (903.02): C, 58.52; H, 4.24; N, 12.41; S, 10.65; Found C, 58.76; H, 4.33; N, 12.69; S, 10.80.

5.1.2.5. 2-[(2-(4-(3-(4-Nitrophenyl)ureido)phenyl)-2-oxoethyl)thio]-1H-benzo[d]imidazol-3-ium sulfate ***8c***. Dark yellow powder, (yield 88%), m.p. 277–280 °C; IR (KBr, ν cm^{-1}): 3217, 3356 (NHs) and 1689 (C=O); ^{1}H NMR (DMSO-d_6) δ *ppm*: 5.29 (s, 4H, 2C$\underline{H}_2$), 7.42–7.45 (m, 4H, Ar−H), 7.66–7.76 (m, 12H, Ar−H), 8.04 (d, 4H, Ar−H, J = 8.8 Hz), 8.22 (d, 4H, Ar−H, J = 9.2 Hz), 9.60 (s, 2H, 2 NH), 9.75 (s, 2H, 2 NH, D_2O exchangeable), 12.51 (s, 2H, 2 NH, D_2O exchangeable); ^{13}C NMR (DMSO-d_6) δ *ppm*: 40.60 ($\underline{C}H_2$), 118.06, 118.15, 118.22, 118.27, 120.25, 121.71, 124.07, 125.59, 129.87, 130.09, 130.42, 141.66, 146.76, 150.26, 152.42, 191.55 (2$\underline{C}$ = O); Anal. Calcd. for $C_{44}H_{36}N_{10}O_{12}S_3$ (993.01): C, 53.22; H, 3.65; N, 14.11; S, 9.69; Found C, 53.49; H, 3.71; N, 14.45; S, 9.82.

5.1.2.6. 2-[(2-Oxo-2-(4-(pyrrolidin-1-yl)phenyl)ethyl)thio]-1H-benzo[d] imidazol-3-ium sulfate ***13a***. Grey crystals, (yield 90%), m.p. 219–221 °C; IR (KBr, ν cm^{-1}): 3421 (NHs) and 1650 (C=O); ^{1}H NMR (DMSO-d_6) δ *ppm*: 1.97–2.00 (m, 8H, pyrrolidine Hs), 3.34–3.37 (m, 8H, pyrrolidine Hs), 5.06 (s, 4H, 2 C$\underline{H}_2$), 6.62 (d, 2H, Ar−H, J = 8.9 Hz), 7.12–7.16 (m, 8H, Ar−H), 7.27–7.29 (m, 2H, Ar−H), 7.54–7.56 (m, 2H, Ar−H), 7.89 (d, 2H, Ar−H, J = 8.9 Hz), 12.51 (s, 2H, 2NH, D_2O exchangeable); ^{13}C NMR (DMSO-d_6) δ *ppm*: 25.38 (pyrrolidine $\underline{C}H_2$), 43.18 ($\underline{C}H_2$), 47.78 (pyrrolidine $\underline{C}H_2$), 109.98, 111.34, 120.20, 122.61, 130.13, 132.67, 139.69, 145.05, 150.37, 151.57, 168.48, 190.88 ($\underline{C}$=O); Anal. Calcd. for $C_{38}H_{40}N_6O_6S_3$ (772.95): C, 59.05; H, 5.22; N, 10.87; S, 12.45; Found C, 58.89; H, 5.38; N, 10.95; S, 12.61.

5.1.2.7. 2-[(2-(4-Morpholinophenyl)-2-oxoethyl)thio]-1H-benzo[d] imidazol-3-ium sulfate ***13b***. Buff crystals, (yield 95%), m.p. 260–262 °C; IR (KBr, ν cm^{-1}): 3421 (NH) and 1643 (C=O); ^{1}H NMR (DMSO-d_6) δ *ppm*: 3.35–3.37 (m, 8H, morpholine Hs), 3.73–3.76 (m, 8H, morpholine Hs), 5.25 (s, 4H, 2 C$\underline{H}_2$), 7.05 (d, 2H, Ar−H, J = 9.1 Hz), 7.11–7.18 (m, 8H, Ar−H), 7.45–7.47 (m, 2H, Ar−H), 7.68–7.70 (m, 2H, Ar−H), 7.92 (d, 2H, Ar−H, J = 9.0 Hz), 12.56 (s, 2H, 2NH, D_2O exchangeable); ^{13}C NMR (DMSO-d_6) δ *ppm*: 41.37 ($\underline{C}H_2$), 47.04, 66.25 (morpholine Cs), 109.98, 113.65, 114.93, 123.10, 125.41, 130.84, 131.05, 133.47, 151.30, 155.11, 168.48, 190.10 ($\underline{C}$=O); ESI MS *m/z*: 804 [M]$^+$; Anal. Calcd. for $C_{38}H_{40}N_6O_8S_3$ (804.95): C, 56.70; H, 5.01; N, 10.44; S, 11.95; Found C, 56.87; H, 4.14; N, 10.67; S, 12.08.

5.1.2.8. 2-[(2-(4-(1H-Imidazol-1-yl)phenyl)-2-oxoethyl)thio]-1H-benzo [d]imidazol-3-ium sulfate ***13c***. Buff powder, (yield 93%), m.p. 245–247 °C; IR (KBr, ν cm^{-1}): 3410 (NH) and 1678 (C=O); ^{1}H NMR (DMSO-d_6) δ *ppm*: 5.36 (s, 4H, 2 C$\underline{H}_2$), 7.13–7.14 (m, 2H, Ar−H), 7.36–7.43 (m, 4H, Ar−H), 7.63–7.68 (m, 4H, Ar−H), 7.99 (s, 2H, Ar−H), 8.08 (d, 4H, Ar−H, J = 8.6 Hz), 8.32 (d, 4H, Ar−H, J = 8.7 Hz), 8.46 (s, 2H, Ar−H), 12.51 (s, 2H, 2NH, D_2O exchangeable); ^{13}C NMR (DMSO-d_6) δ ppm: 41.28 ($\underline{C}H_2$), 109.95, 113.88, 121.09, 121.88, 122.54, 122.77, 124.77, 130.88, 132.71, 134.82, 135.64, 135.77, 139.13, 150.56, 192.13 (C=O); Anal. Calcd. for $C_{36}H_{30}N_8O_6S_3$ (766.87): C, 56.38; H, 3.94; N, 14.61; S, 12.54; Found C, 56.62; H, 3.87; N, 14.89; S, 12.60.

5.1.2.9. 2-[(2-(4-(1H-Benzo[d][1,2,3]triazol-1-yl)phenyl)-2-oxoethyl) thio]-1H-benzo[d]imidazol-3- ium sulfate ***13d***. White powder, (yield 89%), m.p. 260–262 °C; IR (KBr, ν cm^{-1}): 3414 (NH) and 1678 (C=O); ^{1}H NMR (DMSO-d_6) δ *ppm*: 5.41 (s, 4H, 2 C$\underline{H}_2$), 7.42–7.44 (m, 4H, Ar−H), 7.57–7.61 (m, 2H, Ar−H), 7.67–7.69 (m, 4H, Ar−H), 7.74–7.78 (t, 2H, Ar−H, J = 7.6 Hz), 8.07–8.11 (m, 2H, Ar−H), 8.20 (d, 2H, Ar−H, J = 8.7 Hz), 8.26 (d, 2H, Ar−H, J = 8.4 Hz), 8.37 (t, 4H, Ar−H, J = 7.5 Hz), 8.56 (d, 2H, Ar−H, J = 8.8 Hz), 12.52 (s, 2H, 2NH, D_2O exchangeable); ^{13}C NMR (DMSO-d_6) δ *ppm*: 41.15 ($\underline{C}H_2$), 111.73, 113.89, 118.89, 120.92, 122.82, 124.49, 125.67, 128.96, 129.76, 130.96, 131.96, 134.96, 140.87, 146.51, 150.59, 192.16 ($\underline{C}$=O); Anal. Calcd. for $C_{42}H_{32}N_{10}O_6S_3$ (868.96): C, 58.05; H, 3.71; N, 16.12; S, 11.07; Found C, 58.27; H, 3.89; N, 16.34; S, 11.21.

5.1.3. General procedure for preparation of compounds ***4a, b, 9a-c*** *and* ***14a-d***

A suspension of different 2-substituted-benzimidazol-3-ium sulfate salts **3a**, **b**, **8a-c** and **13a-d** (2 mmol) in water (10 mL) was stirred at room temperature with an aqueous solution of sodium bicarbonate overnight. The solid obtained was filtered, washed with water, dried and then crystallized from ethanol to afford the corresponding free bases **4a**, **b**, **9a-c** and **14a-d**, respectively.

5.1.3.1. 2-[(1H-benzo[d]imidazol-2-yl)thio]-1-(benzofuran-2-yl)ethanone ***4a***. Buff powder, (yield 91%), m.p. 170–172 °C; IR (KBr, ν cm^{-1}): 3394 (NH) and 1678 (C=O); ^{1}H NMR (DMSO-d_6) δ *ppm*: 4.96 (s, 2H, C$\underline{H}_2$), 7.09–7.14 (m, 2H, Ar−H), 7.41–7.42 (m, 3H, Ar−H), 7.59 (t, 1H, Ar−H, J = 7.6 Hz), 7.75 (d, 1H, Ar−H, J = 8.3 Hz), 7.88 (d, 1H, Ar−H, J = 7.7 Hz), 8.12 (s, 1H, Ar−H), 12.65 (s, 1H, NH, D_2O exchangeable); ^{13}C NMR (DMSO-d_6) δ ppm: 40.62 ($\underline{C}H_2$), 110.86, 114.96, 117.81, 122.18, 126.61, 129.38, 131.82, 136.03, 143.92, 149.49, 152.36, 154.29, 184.38 (C=O); ESI MS *m/z*: 308 [M]$^+$; Anal. Calcd. for $C_{17}H_{12}N_2O_2S$ (308.35): C, 66.22; H, 3.92; N, 9.08; S, 10.40; Found C, 66.43; H, 4.15; N, 9.23; S, 10.59.

5.1.3.2. 2-[(1H-benzo[d]imidazol-2-yl)thio)-1-(5-bromobenzofuran-2-yl) ethanone ***4b***. White powder, (yield 88%), m.p. 183–185 °C; IR (KBr, ν cm^{-1}): 3380 (NH) and 1685 (C=O); ^{1}H NMR (DMSO-d_6) δ *ppm*: 4.98 (s, 2H, C$\underline{H}_2$), 7.16–7.18 (m, 2H, Ar−H), 7.44–7.47 (m, 2H, Ar−H), 7.71–7.78 (m, 2H, Ar−H), 8.06 (s, 1H, Ar−H), 8.13 (s, 1H, Ar−H), 12.55 (s, 1H, NH, D_2O exchangeable); ^{13}C NMR (DMSO-d_6) δ *ppm*: 38.91 ($\underline{C}H_2$), 109.94, 114.93, 115.54, 121.92, 122.77, 124.69, 127.21, 132.72, 149.59, 151.40, 155.54, 168.60, 184.33 (C=O); ESI MS *m/z*: 387 [M]$^+$; Anal. Calcd. for $C_{17}H_{11}BrN_2O_2S$ (387.25): C, 52.73; H, 2.86; N, 7.23; S, 8.28; Found C, 52.91; H, 3.07; N, 7.45; S, 8.31.

5.1.3.3. 2-[(1H-Benzo[d]imidazol-2-yl)thio]-1-(4-aminophenyl)ethanone ***9a***. White powder, (yield 92%), m.p. 117–120 °C; IR (KBr, ν cm^{-1}): 3471, 3367 (NHs) and 1650 (C=O); ^{1}H NMR (DMSO-d_6) δ *ppm*: 4.87 (s, 2H, C$\underline{H}_2$), 6.20 (s, 2H, NH_2, D_2O exchangeable), 6.60 (d, 2H, Ar−H, J = 8.7 Hz), 7.09–7.11 (m, 2H, Ar−H), 7.41–7.43 (m, 2H, Ar−H), 7.77 (d, 2H, Ar−H, J = 8.7 Hz), 11.00 (s, 1H, NH, D_2O exchangeable); ^{13}C NMR (DMSO-d_6) δ ppm: 40.62 ($\underline{C}H_2$), 113.04, 121.72, 123.29, 125.82,

127.31, 131.41, 150.49, 154.71, 190.71 (C═O); ESI MS *m/z*: 283 $[M]^+$; Anal. Calcd. for $C_{15}H_{13}N_3OS$ (283.35): C, 63.58; H, 4.62; N, 14.83; S, 11.32; Found C, 63.74; H, 4.80; N, 15.12; S, 11.55.

5.1.3.4. 1-[4-(2-((1H-Benzo[d]imidazol-2-yl)thio)acetyl)phenyl]-3-phenylurea ***9b***. White powder, (yield 91%), m.p. 248–250 °C; IR (KBr, ν cm^{-1}): 3352, 3278 (NHs) and 1654 (C═O); ^{1}H NMR (DMSO-d_6) δ *ppm*: 5.29 (s, 2H, C$\underline{H_2}$), 7.00 (t, 1H, Ar−H, *J* = 7.3 Hz), 7.31 (t, 2H, Ar−H, *J* = 7.9 Hz), 7.37–7.39 (m, 2H, Ar−H), 7.48 (d, 2H, Ar−H, *J* = 7.6 Hz), 7.61–7.63 (m, 2H, Ar−H), 7.66 (d, 2H, Ar−H, *J* = 8.8 Hz), 8.04 (d, 2H, Ar−H, *J* = 8.8 Hz), 9.29 (s, 1H, NH, D_2O exchangeable), 9.69 (s, 1H, NH, D_2O exchangeable), 12.52 (s, 1H, NH, D_2O exchangeable); ^{13}C NMR (DMSO-d_6) δ *ppm*: 41.49 (C$\underline{H_2}$), 113.69, 117.49, 118.74, 122.67, 124.85, 128.47, 129.30, 130.64, 134.40, 139.80, 145.95, 150.97, 152.73, 191.07 (2C = O); ESI MS *m/z*: 402 $[M]^+$, 403 $[M + 1]^+$; Anal. Calcd. for $C_{22}H_{18}N_4O_2S$ (402.47): C, 65.65; H, 4.51; N, 13.92; S, 7.97; Found C, 65.89; H, 4.63; N, 14.08; S, 8.19.

5.1.3.5. 1-[4-(2-((1H-Benzo[d]imidazol-2-yl)thio)acetyl)phenyl]-3-(4-nitrophenyl)urea ***9c***. Yellow powder, (yield 95%), m.p. 170–172 °C; IR (KBr, ν cm^{-1}): 3479, 3356 (NHs) and 1662 (C═O); ^{1}H NMR (DMSO-d_6) δ *ppm*: 5.00 (s, 2H, C$\underline{H_2}$), 7.09–7.11 (m, 2H, Ar−H), 7.40–7.42 (m, 2H, Ar−H), 7.67 (d, 2H, Ar−H, *J* = 8.6 Hz), 7.73 (d, 2H, Ar−H, *J* = 9.1 Hz), 8.04 (d, 2H, Ar−H, *J* = 8.4 Hz), 8.20 (d, 2H, Ar−H, *J* = 9.1 Hz), 10.24 (br s, 2H, 2NH, D_2O exchangeable), 12.50 (s, 1H, NH, D_2O exchangeable); ^{13}C NMR (DMSO-d_6) δ *ppm*: 41.28 (C$\underline{H_2}$), 113.69, 118.20, 118.31, 124.09, 125.30, 125.58, 129.08, 129.88, 130.57, 141.85, 145.23, 146.42, 152.19, 191.03 (2C = O); ESI MS *m/z*: 447 $[M]^+$; Anal. Calcd. for $C_{22}H_{17}N_5O_4S$ (447.47): C, 59.05; H, 3.83; N, 15.65; S, 7.17; Found C, 59.31; H, 4.09; N, 15.83; S, 7.24.

5.1.3.6. 2-[(1H-benzo[d]imidazol-2-yl)thio]-1-[4-(pyrrolidin-1-yl)phenyl] ethanone ***14a***. Brown powder, (yield 88%), m.p. 130–132 °C; IR (KBr, ν cm^{-1}): 3275 (NH) and 1635 (C═O); ^{1}H NMR (DMSO-d_6) δ *ppm*: 1.97–2.00 (m, 4H, pyrrolidine Hs), 3.34–3.37 (m, 4H, pyrrolidine Hs), 4.91 (s, 2H, C$\underline{H_2}$), 6.60 (d, 2H, Ar−H, *J* = 8.8 Hz), 7.11–7.14 (m, 2H, Ar−H), 7.37 (d, 1H, Ar−H, *J* = 6.4 Hz), 7.47 (d, 1H, Ar−H, *J* = 7.0 Hz), 7.89 (d, 2H, Ar−H, *J* = 8.8 Hz), 12.56 (s, 1H, NH, D_2O exchangeable); ^{13}C NMR (DMSO-d_6) δ *ppm*: ^{13}C NMR (DMSO-d_6) δ *ppm*: 25.39 (pyrrolidine C$\underline{H_2}$), 43.14 (C$\underline{H_2}$), 47.80 (pyrrolidine C$\underline{H_2}$), 109.94, 111.37, 120.28, 122.77, 130.17, 132.70, 144.98, 151.62, 168.19, 171.74, 190.52 (C═O); ESI MS *m/z*: 337 $[M]^+$; Anal. Calcd. for $C_{19}H_{19}N_3OS$ (337.44): C, 67.63; H, 5.68; N, 12.45; S, 9.50; Found C, 67.80; H, 5.89; N, 12.61; S, 9.63.

5.1.3.7. 2-[(1H-Benzo[d]imidazol-2-yl)thio]-1-(4-morpholinophenyl) ethanone ***14b***. White powder, (yield 86%), m.p. 241–243 °C; IR (KBr, ν cm^{-1}): 3414 (NH) and 1658 (C═O); ^{1}H NMR (DMSO-d_6) δ *ppm*: 3.32 (t, 4H, morpholine Hs, *J* = 4.8 Hz), 3.74 (t, 4H, morpholine Hs, *J* = 4.7 Hz), 4.95 (s, 2H, C$\underline{H_2}$), 7.02 (d, 1H, Ar−H, *J* = 9.0 Hz), 7.11–7.16 (m, 5H, Ar−H), 7.42–7.44 (m, 1H, Ar−H), 7.93 (d, 1H, Ar−H, *J* = 8.9 Hz), 12.52 (s, 1H, NH, v); ^{13}C NMR (DMSO-d_6) δ *ppm*: 40.61 (C$\underline{H_2}$), 47.14, 66.28 (morpholine carbons), 109.93, 113.41, 121.77, 125.54, 130.85, 132.71, 154.81, 168.59, 191.49 (C═O); ESI MS *m/z*: 353 $[M]^+$; Anal. Calcd. for $C_{19}H_{19}N_3O_2S$ (353.44): C, 64.57; H, 5.42; N, 11.89; S, 9.07; Found C, 64.80; H, 5.63; N, 12.15; S, 9.23.

5.1.3.8. 2-[(1H-Benzo[d]imidazol-2-yl)thio]-1-(4-(1H-imidazol-1-yl) phenyl)ethanone ***14c***. Buff powder, (yield 90%), m.p. 228–230 °C; IR (KBr, ν cm^{-1}): 3379 (NH) and 1683 (C═O); ^{1}H NMR (DMSO-d_6) δ *ppm*: 5.08 (s, 2H, C$\underline{H_2}$), 7.10–7.17 (m, 3H, Ar−H), 7.41–7.43 (m, 2H, Ar−H), 7.91 (t, 3H, Ar−H, *J* = 8.3 Hz), 8.21 (d, 2H, Ar−H, *J* = 8.3 Hz), 8.47 (s, 1H, Ar−H), 12.59 (s, 1H, NH, D_2O exchangeable); ^{13}C NMR (DMSO-d_6) δ *ppm*: 40.61 (C$\underline{H_2}$), 109.94, 118.26, 121.86, 122.77, 130.89, 132.71, 133.89, 136.25, 141.04, 149.87, 168.59, 192.89 (C═O); ESI MS *m/z*: 334 $[M]^+$; Anal. Calcd. for $C_{18}H_{14}N_4OS$ (334.39): C, 64.65; H, 4.22; N, 16.75; S, 9.59; Found C, 64.81; H, 4.39; N, 17.03; S, 9.71.

5.1.3.9. 1-[4-(1H-Benzo[d][1,2,3]triazol-1-yl)phenyl]-2-((1H-benzo[d] imidazol-2-yl)thio) ethanone ***14d***. Light yellow powder, (yield 87%), m.p. 220–222 °C; IR (KBr, ν cm^{-1}): 3325 (NH) and 1681 (C═O); ^{1}H NMR (DMSO-d_6) δ *ppm*: 5.09 (s, 2H, C$\underline{H_2}$), 7.07–7.12 (m, 2H, Ar−H), 7.39 (br s, 2H, Ar−H), 7.57 (t, 1H, Ar−H, *J* = 7.1 Hz), 7.73 (t, 1H, Ar−H, *J* = 7.6 Hz), 8.07 (d, 1H, Ar−H, *J* = 8.2 Hz), 8.13 (d, 1H, Ar−H, *J* = 8.4 Hz), 8.24 (d, 1H, Ar−H, *J* = 8.4 Hz), 8.34 (br s, 2H, Ar−H), 8.49 (d, 1H, Ar−H, *J* = 8.4 Hz), 12.52 (s, 1H, NH, D_2O exchangeable); ^{13}C NMR (DMSO-d_6) δ *ppm*: 40.60 (C$\underline{H_2}$), 109.95, 111.71, 114.31, 118.86, 120.40, 121.68, 122.60, 125.58, 128.80, 129.65, 131.98, 133.10, 140.30, 145.27, 146.46, 168.66 (C═O); ESI MS *m/z*: 385 $[M]^+$; Anal. Calcd. for $C_{21}H_{15}N_5OS$ (385.44): C, 65.44; H, 3.92; N, 18.17; S, 8.32; Found C, 65.80; H, 4.06; N, 18.45; S, 8.49.

5.2. Biological evaluation

5.2.1. In vitro anticancer activity as primary single high dose (10^{-5} M) screening

The cytotoxicity assays for compound **4a** were performed according to the protocol of National Cancer Institute (NCI), Bethesda, USA (against 60 cell lines) [30,31]. Drug exposure protocol was applied for 48 h using sulforhodamine B (SRB) protein assay [30] and cell viability and growth was estimated, as reported earlier [22].

5.2.2. In vitro cytotoxic activity against renal cancer cell line A498

A498 cell viability tesing of all the synthesized compounds at conc. 10 μM and consequently IC_{50} values on serial concentrations of the compounds with the best results namely **3a, 4a, 8a, 8c, 9a** and **9c** were determined using MTT spectrophotometric assay. Initial incubation of A498 renal cancer cells was done at 37 °C for 24 h followed by incubation of the desired concentration of each tested compound with the cells for 48 h at 37 °C, then the plates were examined under the inverted microscope and proceeded for the MTT assay according to the reported procedure [32,33].

5.2.2.1. Flowcytometric analysis

5.2.2.1.1. Cell cycle analysis. Further exploration of the cytotoxic activity of compound **4a** was performed using propidium iodide (PI) flow cytomertric analysis to measure the extent of PI that binds to DNA of dead cells with permeable plasma membranes to determine cell cycle status in tissue culture quantitate cell death at all cell phases [34]. After incubation of A498 cells with compound **4a**, cells were fixed with ethanol then dehydrated before staining with PI according to the reported methodology [35].

5.2.2.1.2. Annexin-V FTIC apoptotic study. An apoptotic study using Annexin V-FITC dual staining assay was carried out on compound **4a** at its IC_{50} concentration (6.97 μM) in three successive steps; incubation of cells with Annexin V-FITC followed by quantification by flow cytometry and finally detection by fluorescence microscope according to the published protocol [36].

5.2.2.2. Inhibitory activity of compound ***4a*** *against c-MET kinase*. An ADP-Gl kinase assay measures ADP formed from a kinase reaction. ADP is converted into ATP, which is used to generate light in a luciferase reaction. The luminescence generated correlates with the c-MET kinase activity of compound **4a.** The enzyme and its substrate with ATP and compound **4a** all are buffered and added to the wells and incubated at room temperature for 60 min followed by addition of the ADP-Glo reagent and finally the kinase detection reagent following the steps the documented experimental steps [37].

*5.2.2.3. Inhibitory activity of compound **4a** against MAP kinase.* A time resolved fluorescence resonance energy transfer assay was carried out to determine the MAP kinase inhibitory activity of compound **4a** (LANCE) in two steps. Firstly, kinase reaction step by mixing and incubation of MAP kinase with the ULight-substrate, ATP, and compound **4a** in a suitable buffer and secondly, a detection step according to reported [38].

5.3. In silico studies

5.3.1. Molecular docking simulations

Molecular docking studies were performed using Accelerys software (Discovery Studio 4) for compound **4a** against c-MET kinase (PDB code 3ZZE). Crystal structure (3ZZE) (resolution 1.87 Å) was downloaded and prepared as reported [39]. Ligand was drawn using marvin sketch and imported to the visualizer and prepared as reported [40]. Docking simulations were run using CDOCKER for the co-crystallized ligand and then it was validated by the alignment of the co-crystallized ligand and docked ligand to calculate RMSD value, which was 0.89 Å. The docked poses were ranked according to their cDOCKER interaction energy, and the top pose was chosen for analysis of interactions for each compound.

5.3.2. ADME study and pharmacokinetic properties prediction

The pharmacokinetic data relevant to compound **4a** was achieved via the free online server swissADME (http://swissadme.ch/index.php#undefined) where the SMILE of the compound was inserted directly on the webpage followed by running the prediction process. A whole set of the different physical properties, pharmacokinetic parameters ADME parameters along with the BOILED-Egg chart were obtained online and explained [27,28].

Funding

This research did not receive any specific grant from funding agencies in the public, commercial, or not-for-profit sectors.

Acknowledgment

Authors would show sincere gratitude for the NCI Developmental Therapeutic Program for carrying out the in vitro anticancer screening of compound **8c** on a panal of sixty cell lines.

References

[1] J. Ferlay, I. Soerjomataram, R. Dikshit, S. Eser, C. Mathers, M. Rebelo, D.M. Parkin, D. Forman, F. Bray, Cancer incidence and mortality worldwide: sources, methods and major patterns in GLOBOCAN, Int. J. Cancer 136 (2015) (2012) E359–E386.
[2] P. Lindblad, Epidemiology of renal cell carcinoma, Scand. J. Surg. 93 (2004) 88–96.
[3] M. Mohammadian, R. Pakzad, F. Towhidi, B.R. Makhsosi, A. Ahmadi, H. Salehiniya, Incidence and mortality of kidney cancer and its relationship with HDI (Human Development Index) in the world in 2012, Clujul Med. 90 (2017) 286.
[4] A. Znaor, J. Lortet-Tieulent, M. Laversanne, A. Jemal, F. Bray, International variations and trends in renal cell carcinoma incidence and mortality, Eur. Urol. 67 (2015) 519–530.
[5] P. Cairns, Renal cell carcinoma, Cancer Biomarkers 9 (2011) 461–473.
[6] L.A. Hammond, K. Davidson, R. Lawrence, J.B. Camden, D.D. Von Hoff, S. Weitman, E. Izbicka, Exploring the mechanisms of action of FB642 at the cellular level, J. Cancer Res. Clin. Oncol. 127 (2001) 301–313.
[7] D. Hao, J.D. Rizzo, S. Stringer, R.V. Moore, J. Marty, D.L. Dexter, G.L. Mangold, J.B. Camden, D.D. Von Hoff, S.D. Weitman, Preclinical antitumor activity and pharmacokinetics of methyl-2-benzimidazolecarbamate (FB642), Invest. New Drugs 20 (2002) 261–270.
[8] N. Shrivastava, M.J. Naim, M.J. Alam, F. Nawaz, S. Ahmed, O. Alam, Benzimidazole scaffold as anticancer agent: synthetic approaches and structure-activity relationship, Arch. der Pharm. 350 (2017) e201700040.
[9] P.A. Renhowe, S. Pecchi, C.M. Shafer, T.D. Machajewski, E.M. Jazan, C. Taylor, W. Antonios-McCrea, C.M. McBride, K. Frazier, M. Wiesmann, Design, structure–activity relationships and in vivo characterization of 4-amino-3-benzimidazol-2-ylhydroquinolin-2-ones: a novel class of receptor tyrosine kinase inhibitors, J. Med. Chem. 52 (2008) 278–292.
[10] S. Trudel, Z.H. Li, E. Wei, M. Wiesmann, H. Chang, C. Chen, D. Reece, C. Heise, A.K. Stewart, CHIR-258, a novel, multitargeted tyrosine kinase inhibitor for the potential treatment of t (4; 14) multiple myeloma, Blood 105 (2005) 2941–2948.
[11] H. Joensuu, J.-Y. Blay, A. Comandone, J. Martin-Broto, E. Fumagalli, G. Grignani, X.G. Del Muro, A. Adenis, C. Valverde, A.L. Pousa, Dovitinib in patients with gastrointestinal stromal tumour refractory and/or intolerant to imatinib, Br. J. Cancer 117 (2017) 1278.
[12] B. Chu, F. Liu, L. Li, C. Ding, K. Chen, Q. Sun, Z. Shen, Y. Tan, C. Tan, Y. Jiang, A benzimidazole derivative exhibiting antitumor activity blocks EGFR and HER2 activity and upregulates DR5 in breast cancer cells, Cell Death Dis. 6 (2016) e1686.
[13] H.A. Ibrahim, F.M. Awadallah, H.M. Refaat, K.M. Amin, Design, synthesis and molecular modeling study for some new 2-substituted benzimidazoles as dual inhibitors for VEGFR-2 and c-Met, Future Med. Chem. 10 (2018) 493–509.
[14] H.A. Abdel-Aziz, H.A. Ghabbour, W.M. Eldehna, S.T. Al-Rashood, K.A. Al-Rashood, H.-K. Fun, M. Al-Tahhan, A. Al-Dhfyan, 2-((Benzimidazol-2-yl) thio)-1-arylethan-1-ones: Synthesis, crystal study and cancer stem cells CD133 targeting potential, Eur. J. Med. Chem. 104 (2015) 1–10.
[15] H.A. Abdel-Aziz, W.M. Eldehna, H. Ghabbour, G.H. Al-Ansary, A.M. Assaf, A. Al-Dhfyan, Synthesis, crystal study, and anti-proliferative activity of some 2-benzimidazolylthioacetophenones towards triple-negative breast cancer MDA-MB-468 cells as apoptosis-inducing agents, Int. J. Mol. Sci. 17 (2016) 1221.
[16] F. Sonmez, B. Zengin Kurt, I. Gazioglu, L. Basile, A. Dag, V. Cappello, T. Ginex, M. Kucukislamoglu, S. Guccione, Design synthesis and docking study of novel coumarin ligands as potential selective acetylcholinesterase inhibitors, J. Enz. Inhib Med. Chem. 32 (2017) 285–297.
[17] G.H. Al-Ansary, W.M. Eldehna, H.A. Ghabbour, S.T. Al-Rashood, K.A. Al-Rashood, R.A. Eladwy, A. Al-Dhfyan, M.M. Kabil, H.A. Abdel-Aziz, Cancer stem cells CD133 inhibition and cytotoxicity of certain 3-phenylthiazolo [3, 2-a] benzimidazoles: design, direct synthesis, crystal study and in vitro biological evaluation, J. Enz. Inhib. Med. Chem. 32 (2017) 986–991.
[18] N.P. Buu-Hoï, N.D. Xuong, V. Suu, 573. New NN′-disubstituted thioureas and ureas of biological interest, J. Chem. Soc. (Resumed) (1958) 2815–2821.
[19] P. Magdolen, M. Mečiarová, Š. Toma, Ultrasound effect on the synthesis of 4-alkyl-(aryl) aminobenzaldehydes, Tetrahedron 57 (2001) 4781–4785.
[20] F.-F. Gan, A.A. Nagle, X. Ang, O.H. Ho, S.-H. Tan, H. Yang, W.-K. Chui, E.-H. Chew, Shogaols at proapoptotic concentrations induce G2/M arrest and aberrant mitotic cell death associated with tubulin aggregation, Apoptosis 16 (2011) 856–867.
[21] C.-Y. Yu, C.-L.J. Teng, P.-S. Hung, C.-C. Cheng, S.-L. Hsu, G.-Y. Hwang, Y.-M. Tzeng, Ovatodiolide isolated from Anisomeles indica induces cell cycle G2/M arrest and apoptosis via a ROS-dependent ATM/ATR signaling pathways, Eur. J. Pharmacol. 819 (2018) 16–29.
[22] W.M. Eldehna, M.F. Abo-Ashour, H.S. Ibrahim, G.H. Al-Ansary, H.A. Ghabbour, M.M. Elaasser, H.Y. Ahmed, N.A. Safwat, Novel [(3-indolylmethylene) hydrazono] indolin-2-ones as apoptotic anti-proliferative agents: design, synthesis and in vitro biological evaluation, J. Enz. Inhib. Med. Chem. 33 (2018) 686–700.
[23] G. Gibney, S. Aziz, R. Camp, P. Conrad, B. Schwartz, C. Chen, W. Kelly, H. Kluger, c-Met is a prognostic marker and potential therapeutic target in clear cell renal cell carcinoma, Ann. Oncol. 24 (2012) 343–349.
[24] D. Huang, Y. Ding, W.-M. Luo, S. Bender, C.-N. Qian, E. Kort, Z.-F. Zhang, K. VandenBeldt, N.S. Duesbery, J.H. Resau, Inhibition of MAPK kinase signaling pathways suppressed renal cell carcinoma growth and angiogenesis in vivo, Cancer Res. 68 (2008) 81–88.
[25] J.J. Cui, M. McTigue, M. Nambu, M. Tran-Dubé, M. Pairish, H. Shen, L. Jia, H. Cheng, J. Hoffman, P. Le, Discovery of a Novel Class of Exquisitely Selective Mesenchymal-Epithelial Transition Factor (c-MET) Protein Kinase Inhibitors and Identification of the Clinical Candidate 2-(4-(1-(Quinolin-6-ylmethyl)-1 H-[1, 2, 3] triazolo [4, 5-b] pyrazin-6-yl)-1 H-pyrazol-1-yl) ethanol (PF-04217903) for the Treatment of Cancer, J. Med. Chem. 55 (2012) 8091–8109.
[26] A. Daina, V. Zoete, A BOILED-Egg to predict gastrointestinal absorption and brain penetration of small molecules, ChemMedChem 11 (2016) 1117–1121.
[27] A. Daina, O. Michielin, V. Zoete, SwissADME: a free web tool to evaluate pharmacokinetics, drug-likeness and medicinal chemistry friendliness of small molecules, Sci. Rep. 7 (2017) 42717.
[28] A. Daina, O. Michielin, V. Zoete, iLOGP: a simple, robust, and efficient description of n-octanol/water partition coefficient for drug design using the GB/SA approach, J. Chem. Inf. Model. 54 (2014) 3284–3301.
[29] M.F. Abo-Ashour, W.M. Eldehna, R.F. George, M.M. Abdel-Aziz, M.M. Elaasser, S.M. Abou-Seri, N.M. Abdel Gawad, Synthesis and biological evaluation of 2-aminothiazole-thiazolidinone conjugates as potential antitubercular agents, Future Med. Chem. 10 (2018) 1405–1419.
[30] A. Monks, D. Scudiero, P. Skehan, R. Shoemaker, K. Paull, D. Vistica, C. Hose, J. Langley, P. Cronise, A. Vaigro-Wolff, Feasibility of a high-flux anticancer drug screen using a diverse panel of cultured human tumor cell lines, JNCI, J. Natl. Cancer Inst. 83 (1991) 757–766.
[31] M.R. Boyd, K.D. Paull, Some practical considerations and applications of the National Cancer Institute in vitro anticancer drug discovery screen, Drug Dev. Res. 34 (1995) 91–109.
[32] D.T. Vistica, P. Skehan, D. Scudiero, A. Monks, A. Pittman, M.R. Boyd, Tetrazolium-based assays for cellular viability: a critical examination of selected parameters affecting formazan production, Cancer Res. 51 (1991) 2515–2520.
[33] J.M. Edmondson, L.S. Armstrong, A.O. Martinez, A rapid and simple MTT-based spectrophotometric assay for determining drug sensitivity in monolayer cultures, Methods Cell Sci. 11 (1988) 15–17.

[34] P. Pozarowski, Z. Darzynkiewicz, Analysis of cell cycle by flow cytometry, Checkpoint Controls and Cancer, Springer, 2004, pp. 301–311.
[35] L.C. Crowley, A.P. Scott, B.J. Marfell, J.A. Boughaba, G. Chojnowski, N.J. Waterhouse, Measuring cell death by propidium iodide uptake and flow cytometry, Cold Spring Harbor Protoc. 2016 (2016) pdb. prot087163.
[36] H. Eshghi, M. Hosseini, Selective and convenient protection of aldehydes as azines under solvent-free conditions, J. Chin. Chem. Soc. 55 (2008) 636–638.
[37] J. Alves, S.A. Goueli, H. Zegzouti, P. Corporation, MET (M1250T) Kinase Assay, ADP-Glo™ Kinase Assay Application Notes Tyrosine Kinase Series: MET (M1250T), 1–2.
[38] G. Warner, Measurment of P38/MAPK activity bt LANCETM, Lance Assay Publication Note, 1–8.
[39] W.M. Eldehna, M. Fares, H.S. Ibrahim, M.H. Aly, S. Zada, M.M. Ali, S.M. Abou-Seri, H.A. Abdel-Aziz, D.A.A. El Ella, Indoline ureas as potential anti-hepatocellular carcinoma agents targeting VEGFR-2: synthesis, in vitro biological evaluation and molecular docking, Eur. J. Med. Chem. 100 (2015) 89–97.
[40] H.S. Ibrahim, S.M. Abou-Seri, M. Tanc, M.M. Elaasser, H.A. Abdel-Aziz, C.T. Supuran, Isatin-pyrazole benzenesulfonamide hybrids potently inhibit tumor-associated carbonic anhydrase isoforms IX and XII, Eur. J. Med. Chem. 103 (2015) 583–593.